

## Identifying the effect of aromatic oil on the individual component dynamics of S-SBR/BR blends by broadband dielectric spectroscopy

Rathi, Akansha; Hernandez Santana, M.; Garcia, Santiago J.; Dierkes, Wilma K.; Noordermeer, Jacques W.M.; Bergmann, Cristina; Trimbach, Jürgen; Blume, Anke

**DOI**

[10.1002/polb.24599](https://doi.org/10.1002/polb.24599)

**Publication date**

2018

**Document Version**

Final published version

**Published in**

Journal of Polymer Science. Part B, Polymer Physics

**Citation (APA)**

Rathi, A., Hernandez Santana, M., Garcia, S. J., Dierkes, W. K., Noordermeer, J. W. M., Bergmann, C., Trimbach, J., & Blume, A. (2018). Identifying the effect of aromatic oil on the individual component dynamics of S-SBR/BR blends by broadband dielectric spectroscopy. *Journal of Polymer Science. Part B, Polymer Physics*, 56(11), 842-854. <https://doi.org/10.1002/polb.24599>

**Important note**

To cite this publication, please use the final published version (if applicable).  
Please check the document version above.

**Copyright**

Other than for strictly personal use, it is not permitted to download, forward or distribute the text or part of it, without the consent of the author(s) and/or copyright holder(s), unless the work is under an open content license such as Creative Commons.

**Takedown policy**

Please contact us and provide details if you believe this document breaches copyrights.  
We will remove access to the work immediately and investigate your claim.

# Identifying the Effect of Aromatic Oil on the Individual Component Dynamics of S-SBR/BR Blends by Broadband Dielectric Spectroscopy

Akansha Rathi <sup>1</sup>, Marianella Hernández,<sup>2,3</sup> Santiago J. Garcia,<sup>2</sup> Wilma K. Dierkes,<sup>1</sup> Jacques W. M. Noordermeer <sup>1</sup>, Cristina Bergmann,<sup>4</sup> Jürgen Trimbach,<sup>4</sup> Anke Blume<sup>1</sup>

<sup>1</sup>Department of Elastomer Technology and Engineering, University of Twente, P.O. Box 217, AE Enschede 7500, The Netherlands

<sup>2</sup>Novel Aerospace Materials Group, Faculty of Aerospace Engineering, Delft University of Technology, Kluyverweg 1, 2629 HS Delft, The Netherlands

<sup>3</sup>Institute of Polymer Science and Technology (ICTP-CSIC), Juan de la Cierva 3, Madrid 28006, Spain

<sup>4</sup>Hansen & Rosenthal KG, Am Sandtorkai 64, Hamburg 20457, Germany

Correspondence to: J. W. M. Noordermeer (E-mail: J.W.M.Noordermeer@utwente.nl)

Received 7 December 2017; accepted 22 February 2018; published online 12 March 2018

DOI: 10.1002/polb.24599

**ABSTRACT:** Miscible S-SBR (solution styrene–butadiene copolymer)/BR (polybutadiene homopolymer) blends are used in multiple applications like modern passenger car tire treads. Despite their miscibility, there is a problem to predict tire performance due to dynamical heterogeneities present in the S-SBR/BR blends. On the one hand, S-SBR/BR blends have a thermorheologically complex behavior, which complicates the prediction of the temperature- and frequency-dependence of material properties. On the other hand, due to differences in the polarity of the individual components, the extender oils used in the elastomeric compounds could distribute unequally within the blends, where little is known about how oils interact with the two polymers. In this work a combination of Differential Scanning Calorimetry, Dynamic Mechanical Analysis, and

Broadband Dielectric Spectroscopy (BDS) is used to clarify: (i) the thermorheological complexity of S-SBR/BR blends, (ii) the effect of the extender oil on the blend. The broad frequency operation of BDS allows for the analysis of the S-SBR and BR component dynamics and the effect of the oil on each of them within an S-SBR/BR (50/50) blend. Based on the discretization of individual component dynamics in the blend, conclusive remarks are made on the effect of the extender oil for either component in the blend. © 2018 Wiley Periodicals, Inc. *J. Polym. Sci., Part B: Polym. Phys.* **2018**, *56*, 842–854

**KEYWORDS:** BDS; blends; component dynamics; Differential Scanning Calorimetry; Dynamic Mechanical Analysis; S-SBR/BR

**INTRODUCTION** The outer layer of a tire which establishes the direct contact of the car with the surface of the road and is known as tread, needs to meet high performance requirements. An adequate tire tread performance is commonly achieved by using blends of two or three different types of elastomers. Both miscible and immiscible elastomer blends exhibit dissimilar advantages for tire performance. For example, miscible SBR (styrene–butadiene copolymer)/BR (polybutadiene) blends are used in state-of-the-art tire treads due to the advantageous set of wet-skid resistance, low wear, and low rolling resistance. However, immiscible IR (polyisoprene)/NR (natural rubber) blends are used for improved wet-skid resistance.<sup>1–4</sup>

The low rolling resistance of tire treads composed of miscible SBR/BR blends is typically achieved using chemically coupled silica as reinforcing filler instead of the more traditional physically coupled carbon black.<sup>5</sup> The SBR type is a solution-polymerized SBR (S-SBR) with approximately 50%

of butadiene content in the 1,2-vinyl configuration. The latter is needed to achieve a high enough yield of coupling of the silica with the elastomers by means of sulfur-functional silane coupling agents via a thiol–ene reaction. This radical coupling reaction proceeds particularly well with mercaptosilanes and pendant vinyl-groups.<sup>6</sup> As the glass transition temperature  $T_g$  of high-vinyl S-SBR is too high for tire purposes, it has to be compensated by the admixture of high-cis BR, with a  $T_g$  around  $-90$  to  $-100$  °C. According to thermodynamic predictions and experimental work, vulcanized mixtures of high-vinyl S-SBR and high-cis BR are considered miscible blends at all ratios. Thermodynamically, high-vinyl S-SBR/high-cis BR mixtures increase the positional disorder such that miscibility becomes an entropically favored event.<sup>7–10</sup> The experimental detection of just one  $\tan \delta$  peak in Dynamic Mechanical Analysis (DMA) as well as one single  $T_g$  by Differential Scanning Calorimetry (DSC) indicates homogeneity. Nevertheless, and despite the aforementioned

**TABLE 1** Reported Properties of S-SBR, BR, and TDAE Oil

	S-SBR	BR	TDAE
Styrene (wt%)	21	–	–
1,2-vinyl butadiene (%)	50	<1	–
<i>cis</i> -1,4 butadiene (%)	29 <sup>a</sup>	>96	–
<i>trans</i> -1,4 butadiene (%)		~2	–
Weight average molecular weight ( $M_w$ ) (kg mol <sup>-1</sup> )	475	460	–
Number average molecular weight ( $M_n$ ) (kg mol <sup>-1</sup> )	315	135	–
Glass transition temperature ( $T_g$ ) (°C)	–25	–109	–49

<sup>a</sup> 29% is the combined contribution of *cis*-1,4 and *trans*-1,4 in the S-SBR microstructure.

**TABLE 2** Rubber Formulations

Component	BR (phr)	S-SBR (phr)	S-SBR/BR (phr)
BR	100	–	50
S-SBR	–	100	50
Zinc oxide (ZnO)	4	4	4
Stearic acid (SA)	3	3	3
<i>N</i> -cyclohexyl-2-benzothiazole sulfenamide (CBS)	2.5	2.5	2.5
Sulfur (S)	1.6	1.6	1.6
Treated Distillate	0/10/20	0/10/20	0/10/20
Aromatic Extract (TDAE)			

justifications, the term “miscible blend” should be used with caution. As will be highlighted in more detail hereunder, the judgment on miscibility depends to a large extent on the

**TABLE 3** Mixing Protocol

1st Stage: Internal Mixer Brabender Plasticorder 350S Rotor Speed: 50 RPM; Set Temperature: 50 °C; Fill Factor: 0.7			2nd Stage: Two-Roll Mill Polymix 80T Friction Ratio: 1.25:1 ca. 40 °C All compounds
BR_0	BR_10	BR_20	
S-SBR_0	S-SBR_10	S-SBR_20	
S-SBR/BR_0	S-SBR/BR_10	S-SBR/BR_20	
(min sec)	(min sec)	(min sec)	(min sec)
0.30 Add polymers	0.30 Add polymers	0.30 Add polymers	0.30 Add curatives
1.30 Add ZnO and SA	1.30 Add ZnO and SA	1.30 Add ZnO and SA	(CBS+S)
4.00 Discharge	2.40 Add 3/4th TDAE	2.40 Add 3/8th TDAE	5.00 Discharge
	5.00 Add 1/4th TDAE	5.00 Add 3/8th TDAE	
	7.00 Discharge	8.00 Add 1/4th TDAE	
		10.30 Discharge	

length scale probed by the experimental technique. DSC probes at a frequency of approximately 10<sup>-2</sup> Hz, whereas DMA typically operates at a range of frequencies between 10<sup>-2</sup> and 10<sup>2</sup> Hz. Techniques, such as Broadband Dielectric Spectroscopy (BDS) and Nuclear Magnetic Resonance (NMR) Spectroscopy, have a much broader operation frequency ranging from 10<sup>-2</sup> to 10<sup>10</sup> Hz. This allows detecting a broader range of molecular length scales from less than 1 nm (approximate length scale of a monomer) to almost 100 nm (approximate length scale of a whole polymer chain).<sup>11–25</sup> It might therefore be possible to identify the relaxation times related to either component/blended chains in miscible blends. This possibility was already described in literature as “Concentration Fluctuations (CF)” that can be identified by local variations in relaxation times around an average value in the length scale of approximately 3 nm. Techniques, such as NMR and BDS, are usually employed to study the maximum relaxation time at  $T_g$  ( $\tau_{max}(T_g)$ ) of individual components in so-called miscible blends,<sup>26,27</sup> and may offer an opportunity to evaluate the effect of an oil in each component of a miscible blend.

The two main challenges associated with making a miscible S-SBR/BR blend design with predictable properties are:

(i) The thermorheological complexity which arises due to a large difference of approximately 80 °C in the  $T_g$  of S-SBR and BR. Its major consequence is that the distinct temperature dependencies of the relaxation times of each component start expressing at length scales of about 3 nm. A thermorheologically simple polymer system is one in which the molecular mechanisms contributing to time and frequency dependent modulus and compliance functions have the same temperature dependence.<sup>27</sup> Due to the thermorheological complexity of the blends under consideration, the Time-Temperature Superposition (TTS) concept cannot be applied for predicting the frequency dependence of the modulus, which is the basis for predicting the performance of a tire tread in a dynamic, variable frequency environment. This is of

**TABLE 4** Vulcanization Times as Obtained from the Curing Curves from RPA Measurements

Compound	$t_{c,90}$ (min)
BR_0	18
BR_10	17
BR_20	17
S-SBR_0	23
S-SBR_10	32
S-SBR_20	30
S-SBR/BR_0	19
S-SBR/BR_10	20
S-SBR/BR_20	21

particular importance for the prediction of Wet Skid Resistance (WSR), which is a high frequency ( $10^3$ – $10^6$  Hz) phenomenon.<sup>28</sup>

(ii) The lack of knowledge about the influence of processing chemicals and other compounding ingredients in the S-SBR/BR blend. As there is a polarity difference between S-SBR and BR, it is likely that the processing chemicals such as extender oil may affect one or the other component more based on the “like dissolves like” principle. An indication for such a differing influence can be obtained by studying the effect of the process oil on the maximum relaxation time at  $T_g$  ( $\tau_{\max}(T_g)$ ) of the individual blend components S-SBR and BR.

In this work, the applicability of BDS is explored to understand the effect of Treated Distillate Aromatic Extract (TDAE) mineral-based aromatic extender oil on the two components of an S-SBR/BR (50/50 wt% ratio) blend. For the analysis three TDAE contents, 0/10/20 phr (parts per hundred rubber) are used. The analysis is completed with DSC and DMA. The BDS specific analyses include the use of one or two Havriliak–Negami equations and a procedure for the selection of the most appropriate fitting in these blends.

## EXPERIMENTAL

### Materials

The materials used in this study are S-SBR: SPRINTAN™ SLR 4602 (Trinseo Deutschland GmbH, Schkopau, Germany); BR: BUNA CB24 (Arlanxeo Deutschland GmbH, Leverkusen, Germany); and Treated Distillate Aromatic Extract (TDAE): VIVATEC 500 (Hansen & Rosenthal KG, Hamburg, Germany). Some important analytical properties of S-SBR, BR, and TDAE are presented in Table 1. The curing system employed consists of zinc oxide (ZnO), stearic acid (SA), and sulfur (S) from Sigma Aldrich (St. Louis, MO), and *N*-cyclohexyl-2-benzothiazole sulfenamide (CBS) from Flexys (Brussels, Belgium). All chemical reagents were used as received.

### Mixing

The basic formulation used for this study is presented in Table 2, expressed in parts per hundred parts of rubber

(phr). The compounds were prepared following a 2-step mixing procedure, with a first stage in an internal mixer.

The vulcanization system (CBS + S) was added to the mix in a second stage, carried out on a two-roll mill (Table 3). The compounds are referred to as BR<sub>x</sub>, S-SBR<sub>x</sub>, and S-SBR/BR<sub>x</sub> phr, where “x” corresponds to the amount of TDAE added to the formulations (0/10/20 phr).

### Curing

The samples were vulcanized in a hydraulic press (Wickert WLP 1600) at 100 bar and 160 °C as sheets with a thickness of 2 mm, according to their  $t_{c,90} + 2$  min optimum vulcanization times (see Table 4). The  $t_{c,90}$  was determined with a Rubber Process Analyzer (RPA 2000, Alpha Technologies) following ISO 3147:2008 at 160 °C. 0.1–0.2 mm thick sheets were also vulcanized according to their respective  $t_{c,90}$  values at 160 °C for BDS measurements.

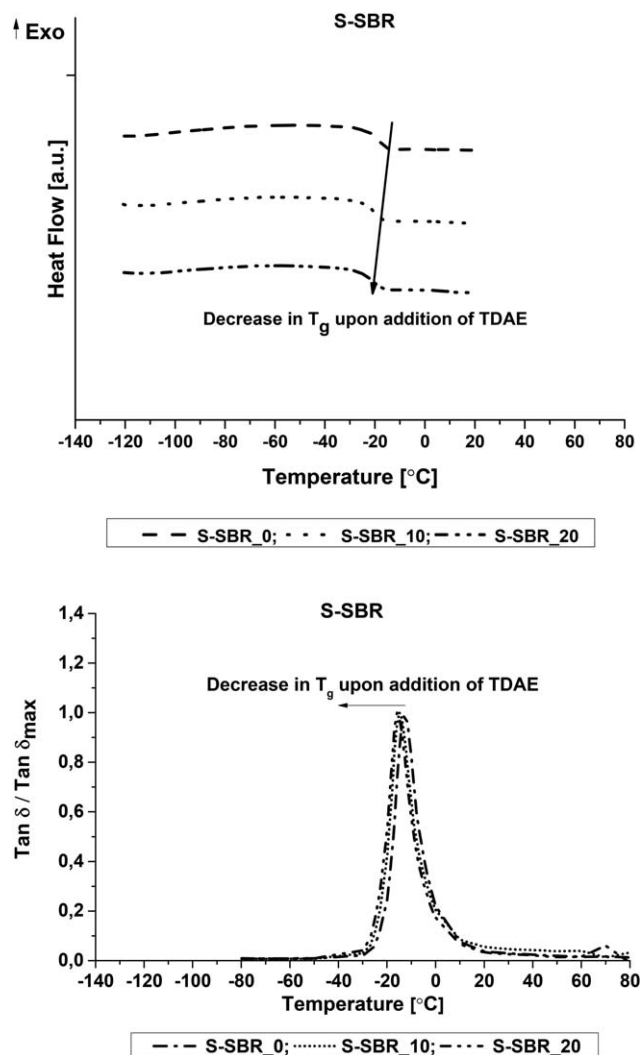


**FIGURE 1** DSC and  $\tan \delta / \tan \delta_{\max}$  curves versus temperature for the S-SBR compounds with different contents of TDAE oil.  $\tan \delta$  values are reported as normalized to their maximum for ease of comparison.

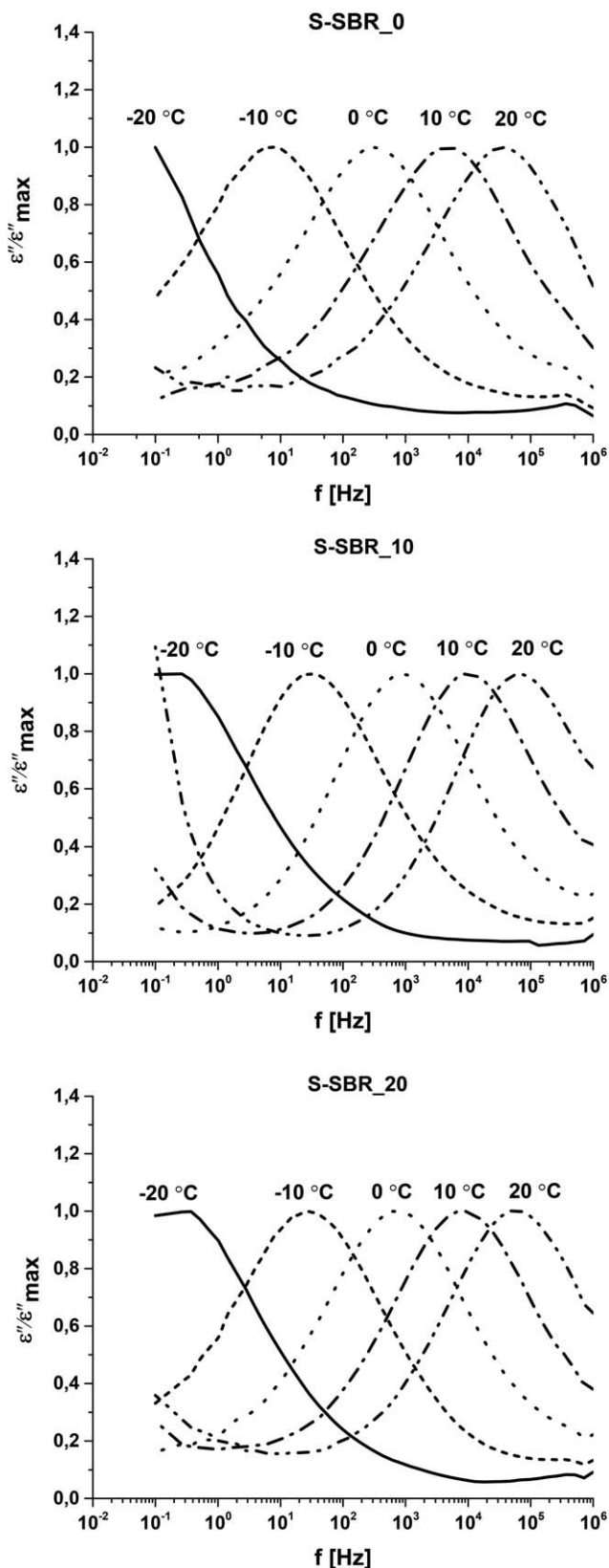


FIGURE 2 Normalized  $\epsilon''$  versus frequency in the region of the  $\alpha$ -relaxation for the S-SBR compounds with different contents of TDAE oil.

### Differential Scanning Calorimetry

A Differential Scanning Calorimeter (DSC) (Perkin Elmer DSC 8000) was used to obtain the “calorimetric” glass transition temperature of the vulcanized samples, using a heating rate of 10 °C/min after quenching to  $-150$  °C, up to 20 °C. The enthalpy precision of the equipment was  $\pm 0.05\%$  to 0.2%. The mid-point of the transition was taken as the value of calorimetric  $T_g$ . The accuracy of the determination was  $\pm 1$  °C in each case.

### Dynamic Mechanical Analysis

Dynamic Mechanical Analysis (DMA) of the vulcanized samples was done in tension mode in a dynamic spectrometer (Metravib DMA 2000) to measure the “dynamic” glass transition temperature. The measurements were performed from  $-150$  °C to  $+80$  °C in steps of 5 °C at a dynamic strain of 0.5% and frequency of 1 Hz on samples of (25\*5\*2) mm. The accuracy of the temperature controller is  $\pm 0.1$  °C, phase angle is  $\pm 0.1^\circ$  and frequency is  $\pm 0.01\%$ . The accuracy of the determination of  $T_g$  was  $\pm 1$  °C in each case.

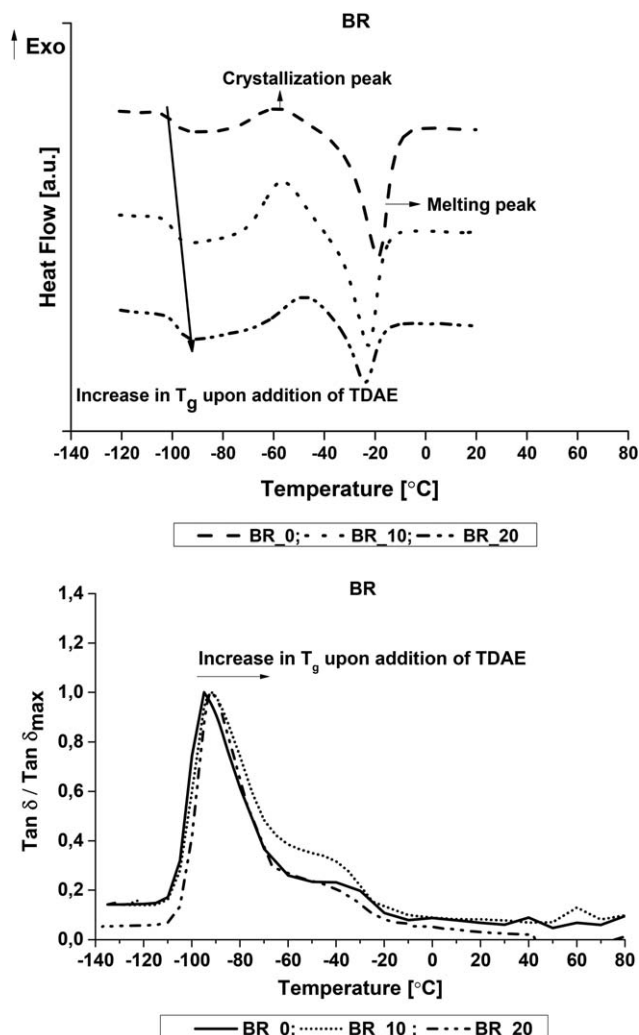
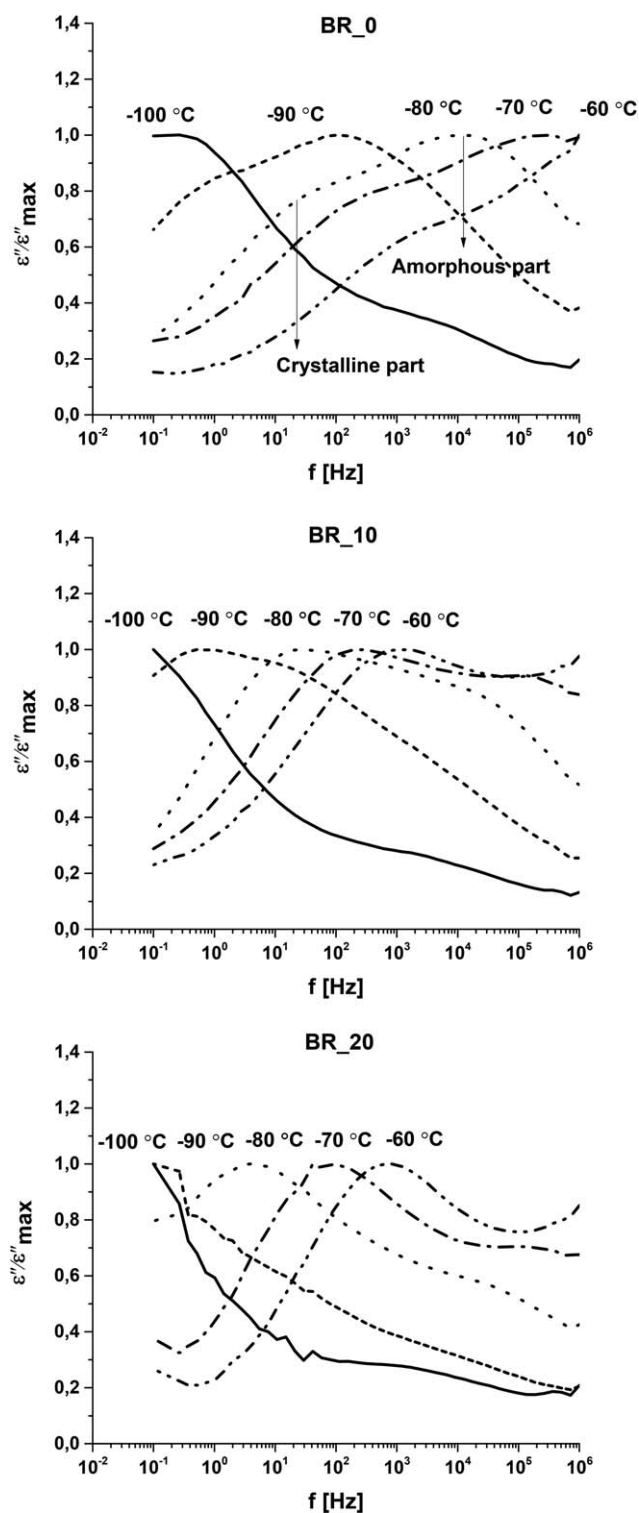


FIGURE 3 DSC and  $\tan \delta / \tan \delta_{\max}$  curves versus temperature for the BR compounds with different contents of TDAE oil.



**FIGURE 4** Normalized  $\epsilon''$  versus frequency in the region of the  $\alpha$ -relaxation for the BR compounds with different contents of TDAE oil.

### Broadband Dielectric Spectroscopy

Broadband Dielectric Spectroscopy (BDS) measurements were performed on a spectrometer with an ALPHA-A High Performance Frequency Analyzer (Novocontrol Technologies). The

vulcanized 0.1–0.2 mm sheets were cut in a disk shape and were mounted in the dielectric cell between two parallel gold plated electrodes. The complex dielectric permittivity  $\epsilon^*$  ( $\epsilon^* = \epsilon' - i\epsilon''$ ), being composed of  $\epsilon'$  as the real part and  $\epsilon''$  the imaginary part, was measured by performing consecutive isothermal frequency sweeps ( $10^{-1}$ – $10^6$  Hz) in the temperature range from  $-120$  °C to  $+80$  °C in steps of  $5$  °C. The temperature was controlled to better than  $0.1$  °C with a Novocontrol Quatro cryosystem; the error of the ALPHA impedance measurement was less than 1%.

## RESULTS AND DISCUSSIONS

### Effect of TDAE on the Individual Polymers: S-SBR and BR, and S-SBR/BR (50/50) Blends

#### S-SBR and BR

A single transition corresponding to  $T_g$  of S-SBR and BR can be observed via DSC, DMA, and BDS (Figs. 1–4). Through DSC and DMA, there is a decrease in  $T_g$  for S-SBR (Fig. 1), and an increase in  $T_g$  upon addition of TDAE for BR (Fig. 3).

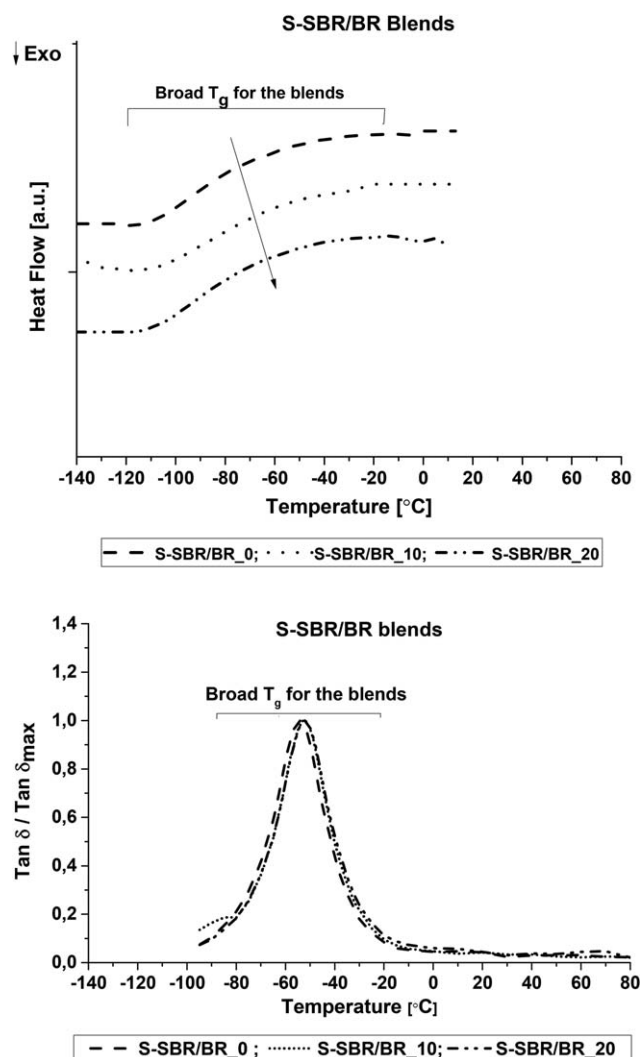


**FIGURE 5** DSC and  $\tan \delta / \tan \delta_{\max}$  curves versus temperature for the S-SBR/BR blends with different contents of TDAE oil.

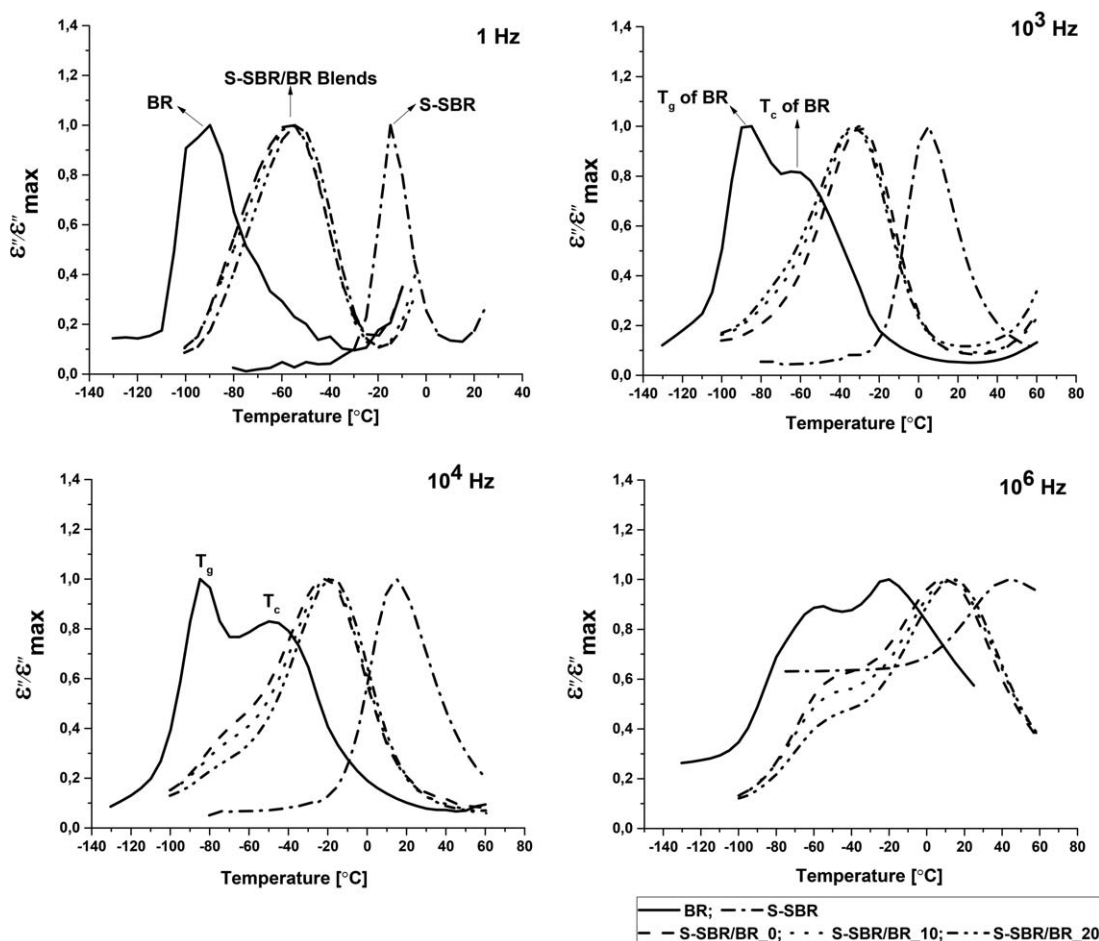


**FIGURE 6** Normalized ( $\epsilon''$ ) versus temperature at 1,  $10^3$ ,  $10^4$ , and  $10^6$  Hz for individual polymers: S-SBR and BR; and for the blends S-SBR/BR with different contents of TDAE oil.  $\epsilon''$  values are reported as normalized to their maxima for ease of comparison.

For BR, a distinct crystallization peak can be seen between  $-60$  and  $-40$  °C due to the ability of the long chain molecules within high-cis content BR to rearrange and form a spherulitic morphology.<sup>29</sup> This crystallinity can be seen in the DSC curve as an exothermic peak between  $-60$  and  $-40$  °C and in the DMA curve as a shoulder on the right-hand side.<sup>29-31</sup> Because the samples were cooled to  $-150$  °C before the DSC measurement, both crystallization and melting peaks are detected. 10 phr TDAE is seen to increase the crystallization enthalpy and reduce the melting enthalpy, while 20 phr TDAE decreases both enthalpies. This effect is attributed to the lack of diluting effect of 10 phr TDAE, while higher TDAE contents (between 10 and 20 phr) seem to have a dissolution effect thereby increasing the local mobility of the BR chains and decreasing the energy needed for the transitions to take place. This effect can also be qualitatively seen from the evaluation of the DSC curve as crystallization being half-way between the  $T_g$  and the melting temperature ( $T_m$ ): crystallization enthalpies of 10, 15, and 8 J/g and melting enthalpies of 20, 16, and 8 J/g for the BR 0, 10, and 20 phr TDAE content, respectively. However, these values should be treated with caution because the experiments were done in a transient mode and not especially designed for studying this phenomenon.<sup>32</sup>

The same crystallinity of BR could also be identified with BDS in both the frequency and temperature domains (Figs. 4 and 6). On the frequency domain curves (Fig. 4), the shoulder is observed on the left side (i.e., lower frequency) of the  $T_g$ , because the relaxations taking place at the surface of the BR microcrystals are slowed down due to surface interactions compared to the more mobile amorphous polymer chains. While on the temperature domain curves (Fig. 6), the crystallinity can be seen as a shoulder on the right side of the  $\epsilon''$  peak. This shoulder moves to higher temperature and increases in intensity, as the frequency is increased.

#### S-SBR/BR Blends

Figure 5 shows a single broad transition corresponding to  $T_g$  for the S-SBR/BR blends, thereby giving a common indication of their miscibility. Similar results were obtained by Shi et al. for analogous SBR/BR blends.<sup>33,34</sup> It is seen that because of the change in the local environment of the blended BR and S-SBR chains, there is hindrance in nuclei formation for the crystallization of the BR chains. In agreement with that, the segmental relaxation corresponding to  $T_g$  is clearly observed by BDS as a broad and asymmetric dielectric loss ( $\epsilon''$ ) peak (Figs. 6 and 7).

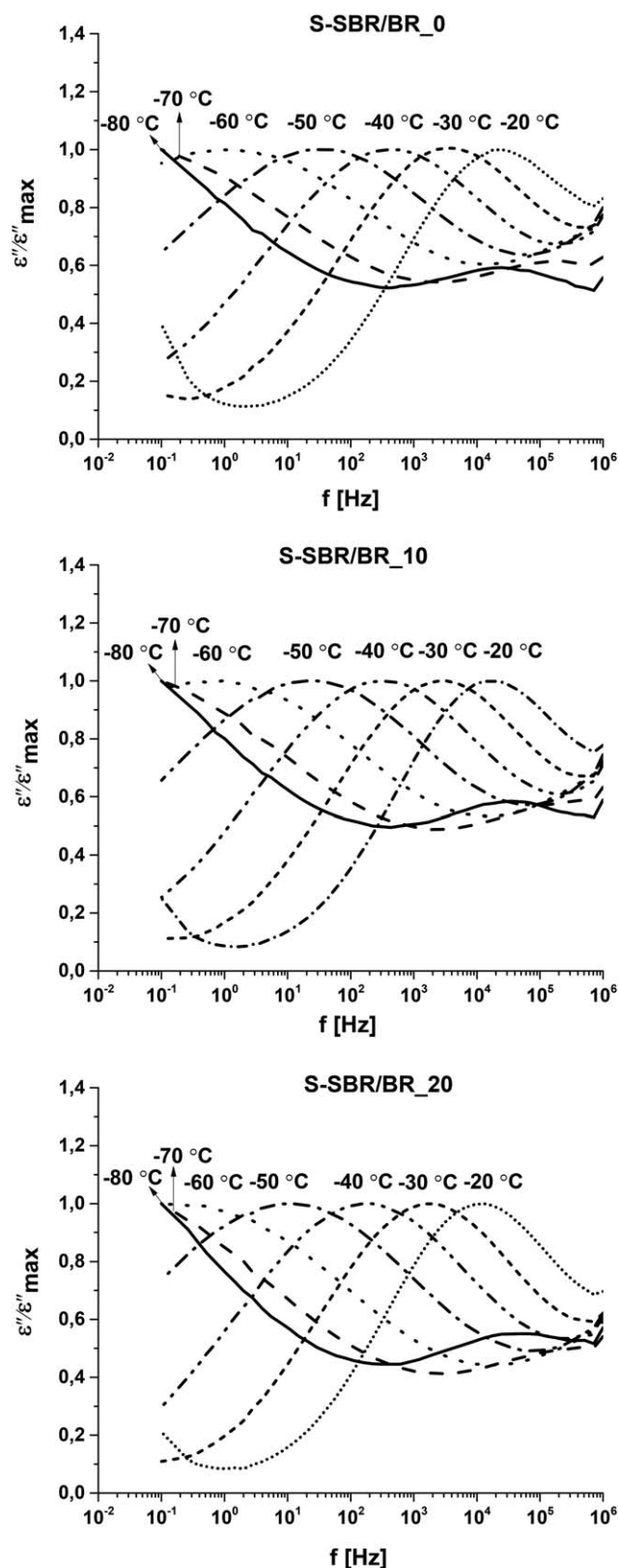


**FIGURE 7** Normalized  $\epsilon''$  versus frequency in the region of the  $\alpha$ -relaxation for the S-SBR/BR blends, with different contents of TDAE oil.

**TABLE 5** HN-Fitting Parameters with One Single HN Equation of S-SBR Individual Polymer with Varying Concentrations of TDAE Oil. The TDAE Oil Parameters are Also Included

Compound	S-SBR_0	S-SBR_10	S-SBR_20	TDAE
$T = -10\text{ }^{\circ}\text{C}$				
$\Delta\epsilon$	0.035	0.19	0.017	0.44
$\tau_{\text{HN}}$ (s)	$3.77 \times 10^{-2}$	$1.39 \times 10^{-2}$	$7.9 \times 10^{-3}$	$1.26 \times 10^{-4}$
$b$	0.54	0.58	0.49	0.69
$c$	0.68	0.57	0.84	0.59
$T = 0\text{ }^{\circ}\text{C}$				
$\Delta\epsilon$	0.035	0.18	0.015	0.40
$\tau_{\text{HN}}$ (s)	$6.01 \times 10^{-4}$	$3.95 \times 10^{-4}$	$2.30 \times 10^{-4}$	$1.59 \times 10^{-5}$
$b$	0.48	0.57	0.49	0.73
$c$	0.90	0.63	0.97	0.56
$T = 10\text{ }^{\circ}\text{C}$				
$\Delta\epsilon$	0.035	0.17	0.015	0.38
$\tau_{\text{HN}}$ (s)	$3.40 \times 10^{-5}$	$3.20 \times 10^{-5}$	$1.89 \times 10^{-5}$	$3.13 \times 10^{-6}$
$b$	0.46	0.56	0.47	0.75
$c$	1	0.66	1	0.54

On the frequency domain curves (Fig. 7), the maximum of the dielectric loss moves to higher frequencies for all systems as the temperature increases, suggesting that this relaxation is due to a thermally activated process.<sup>35</sup> Besides, the broad relaxation becomes narrower as the temperature is increased, which is a characteristic of miscible blends.<sup>14,36</sup> The broadness of the relaxation peaks in the blends increases with the addition of TDAE oil. At a reference temperature of  $-20\text{ }^{\circ}\text{C}$  the width is approximately 5.8 decades for S-SBR/BR\_0 and a bit broader that is, 6.0 decades for the

**TABLE 6** HN-Fitting Parameters with One Single HN Equation of BR Individual Polymer with Varying Concentrations of TDAE Oil

Compound	BR_0	BR_10	BR_20
$T = -90\text{ }^{\circ}\text{C}$			
$\Delta\epsilon$	0.25	0.97	0.65
$\tau_{\text{HN}}$ (s)	$7.38 \times 10^{-4}$	$1.14 \times 10^{-1}$	$8.23 \times 10^0$
$b$	0.34	0.19	1
$c$	0.57	1	0.11
$T = -80\text{ }^{\circ}\text{C}$			
$\Delta\epsilon$	0.23	0.88	0.63
$\tau_{\text{HN}}$ (s)	$9.55 \times 10^{-6}$	$4.72 \times 10^{-4}$	$2.32 \times 10^{-1}$
$b$	0.31	0.20	0.77
$c$	1	1	0.10
$T = -70\text{ }^{\circ}\text{C}$			
$\Delta\epsilon$	0.21	0.85	0.64
$\tau_{\text{HN}}$ (s)	$3.55 \times 10^{-7}$	$3.94 \times 10^{-5}$	$2.21 \times 10^{-2}$
$b$	0.26	0.18	0.64
$c$	0.99	1	0.16

**TABLE 7** HN-Fitting Parameters with One Single HN Equation of S-SBR/BR Blends with Varying Concentrations of TDAE Oil

Compound	S-SBR/BR_0	S-SBR/BR_10	S-SBR/BR_20
<i>T</i> = -40 °C			
$\Delta\epsilon$	0.27	0.81	0.37
$\tau_{\text{HN}}$ (s)	$4.33 \times 10^{-3}$	$8.16 \times 10^{-3}$	$9.12 \times 10^{-3}$
<i>b</i>	0.35	0.40	0.40
<i>c</i>	0.42	0.35	0.39
<i>T</i> = -30 °C			
$\Delta\epsilon$	0.25	0.74	0.36
$\tau_{\text{HN}}$ (s)	$3.85 \times 10^{-4}$	$4.81 \times 10^{-4}$	$6.77 \times 10^{-4}$
<i>b</i>	0.41	0.42	0.42
<i>c</i>	0.40	0.41	0.44
<i>T</i> = -20 °C			
$\Delta\epsilon$	0.25	0.74	0.35
$\tau_{\text{HN}}$ (s)	$7.67 \times 10^{-5}$	$8.53 \times 10^{-5}$	$9.76 \times 10^{-5}$
<i>b</i>	0.48	0.49	0.48
<i>c</i>	0.29	0.32	0.39

S-SBR/BR\_10 and S-SBR/BR\_20 phr TDAE. This marginal effect was expected based on the dynamic heterogeneities increase on the addition of TDAE oil and was not further considered in the discussion.

Even though the miscibility is verified in the studied compounds, polymer blends are practically never fully mixed on a molecular level, especially when the component  $T_g$ 's are more than 50–70 °C apart, as in this case. The reason for the observed indications for miscibility is that eventual heterogeneities are of smaller scale than the sensitivity ranges of DSC and DMA, which makes them unidentifiable through these techniques. On the temperature domain BDS curves (Fig. 6), it is seen that the single, broad transition starts to split into two peaks as the frequency is increased. Up to  $10^3$  Hz, the normalized  $\epsilon''$  peak moves to higher temperatures with increase in frequency, as can be expected based on the Williams-Landel-Ferry (WLF) description of the TTS-principle for a thermorheologically simple polymer system. The deviation from the thermorheological simplicity starts appearing at  $10^4$  Hz, where a shoulder begins to form on the lower temperature side of the normalized  $\epsilon''$  peak. This shoulder becomes more apparent as the frequency is increased, distinguishing smaller scale heterogeneities. In addition, the shoulder at  $10^6$  Hz is at the same position as the  $T_g$  of pristine BR. This suggests that the shoulder corresponds to the BR component of the blend, which tends to disassociate when the length scale of the experimental probe is small enough to detect the relatively shorter relaxation time of BR. Based on the description of dynamic heterogeneities in miscible blends by different theoretical models, the main normalized loss peak can then be associated with the blended segments experiencing a blend environment: slow dynamics, and the shoulder as predominantly BR segments: fast dynamics.<sup>14,37–43</sup> Hereafter, these phases will be called the slow

process and the fast process, respectively. The higher intensity at high frequencies of the blend-rich environment is due to the activation of the rotational and vibrational motions of the styrene groups on the S-SBR chains.

**Effect of TDAE Oil on the Individual Components of the S-SBR/BR Blends: Havriliak–Negami Analysis**

The frequency-domain dielectric data can be further analyzed by fitting the complex dielectric function  $\epsilon^*(\omega)$  with empirical relaxation functions of the Havriliak–Negami (HN) type. The HN equation is a phenomenological expression which can describe a dielectric relaxation process in terms of a characteristic relaxation time at the frequency of the maximum loss.<sup>43</sup> It reads as follows:

$$\epsilon_{\text{HN}}^*(\omega) = \epsilon_\infty + \frac{\Delta\epsilon}{[1 + (i\omega\tau_{\text{HN}})b]c} \quad (1)$$

where  $\tau_{\text{HN}}$  is the characteristic HN relaxation time, which represents the most probable relaxation time from the relaxation time distribution function,  $\omega$  is the angular frequency,  $\Delta\epsilon$  is the relaxation strength ( $\Delta\epsilon = \epsilon_s - \epsilon_\infty$ ), where  $\epsilon_\infty$  and  $\epsilon_s$  are related to the limiting behavior of the complex dielectric function at low and high frequencies respectively,  $\epsilon_{\text{HN}}^*(\omega)$  is the frequency dependent Havriliak–Negami complex dielectric permittivity, and *b* and *c* are shape parameters, which describe the symmetric and asymmetric broadening of the relaxation time distribution function, respectively.

The individual polymers (BR and S-SBR) with and without oil, being composed of single polymeric contributions, are described with one HN equation. Since S-SBR/BR blends with and without TDAE oil are multicomponent systems, two

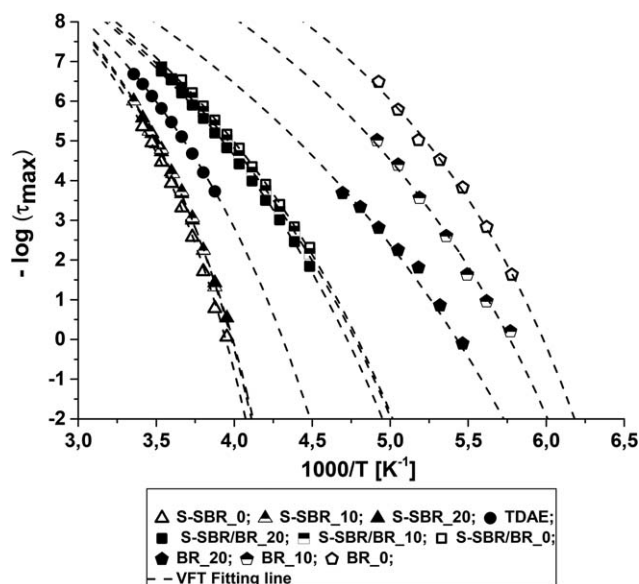


**FIGURE 8** Temperature dependence of the relaxation times at maximum loss of the individual polymers: S-SBR, BR, and S-SBR/BR blends, with varying contents of TDAE oil. The curve corresponding to TDAE oil has been added for the ease of comparison.

**TABLE 8**  $T_g$  at  $\tau_{\max} = 100$  s and 1 s of the Individual Polymer, the TDAE Oil, and the S-SBR/BR Blends with and Without Oil Experimentally Obtained from BDS Measurements

Compound	$T_g$ (100 s) (°C)	$T_g$ (1 s) (°C)	$T_g$ (DSC) (°C)	$T_g$ (Fox Eqn) (°C)	$\Delta T_g$ (100 s) (°C)	$\Delta T_g$ (Fox Eqn) (°C)
S-SBR_0	-27	-20	-30	-	-	-
S-SBR_10	-29	-21	-31	-29	2	2
S-SBR_20	-30	-22	-32	-31	3	4
BR_0	-111	-106	-113	-	-	-
BR_10	-106	-100	-111	-106	5	5
BR_20	-100	-90	-106	-101	11	10
TDAE oil	-50	-41	-49	-	-	-
S-SBR/BR_0	-74	-64	-87	-	-	-
S-SBR/BR_10	-73	-63	-87	-72	1	2
S-SBR/BR_20	-71	-61	-85	-70	3	4

$\Delta T_g$  is calculated w.r.t. BR\_0, S-SBR\_0, S-SBR/BR\_0 value respectively, at 100 s.

approaches have been chosen for the further analysis of these systems: (i) one HN equation to describe the blended S-SBR and BR system; (ii) two HN equations to describe each process from the individual polymeric contributions of S-SBR and BR in the blend.

#### Single HN Equation Based Fittings

The experimental  $\epsilon''$  versus frequency spectra for the individual polymers: S-SBR, BR, and S-SBR/BR blends with and without oil obtained from BDS were fitted using the HN equation. The resulting characteristic parameters  $\Delta\epsilon$ ,  $b$ ,  $c$ , and  $\tau_{\text{HN}}$  are presented in Tables (5–7) with a relative error of less than 4%.  $\Delta\epsilon$  is related to the number density of the polarizable species between the electrodes, depending on many experimental factors such as sample thickness, pressure, and contact area. Because the emphasis in this work is on the location of the  $T_g$  as related to  $\tau_{\text{HN}}$ , being independent of these factors, the  $\Delta\epsilon$  is to be considered as an adjustable parameter in the HN analysis.

The trend in  $\tau_{\text{HN}}$  with the addition of 10 and 20 phr of TDAE oil for all systems, as seen in Tables (5–7) were employed for further analysis as explained below.  $\tau_{\text{HN}}$  is related to the relaxation time of maximum loss,  $\tau_{\max}$  and the frequency of maximum loss,  $f_{\max}$  by the following equation:<sup>44</sup>

$$\tau_{\max} = \frac{1}{2\pi f_{\max}} = \tau_{\text{HN}} \left[ \sin \frac{b\pi}{2+2c} \right]^{-\frac{1}{b}} \left[ \sin \frac{bc\pi}{2+2c} \right]^{\frac{1}{b}} \quad (2)$$

The corresponding values of  $\tau_{\max}$ , plotted in Figure 8, reveal the Vogel–Fülcher–Tamman (VFT) dependence of  $\tau_{\max}$  on the reciprocal temperature as:<sup>45–47</sup>

$$\tau_{\max} = \tau_0 \exp\left(\frac{B}{T-T_0}\right) \quad (3)$$

where  $\tau_0$  and  $B$  are empirical parameters, and  $T_0$  is called the ideal glass transition or Vogel temperature, which is

generally 30–70 K below  $T_g$ .<sup>45</sup> A universal value of  $\log \tau_0 = -14$  was adapted for the data fitting using the VFT equation, based on the relationship of  $\tau_0$  with the  $C_1$  ( $\sim 17$ ) universal parameter from the WLF equation.<sup>48</sup>

The corresponding  $T_g$  for each system is listed in Table 8 calculated as the temperature at  $\tau_{\max} = 100$  s ( $\sim 10^{-2}$  Hz), which is the convention for estimating  $T_g$  by BDS.<sup>49</sup> The temperature corresponding to  $\tau_{\max} = 1$  s ( $\sim 1$  Hz) is also reported in Table 8, since the extrapolation to 100 s can sometimes be misleading, as it is far from the experimentally obtained results.<sup>50</sup> For the systems studied, the values obtained for 100 s and 1 s are very complimentary and hold a similar trend. The comparisons henceforth in this study will be based on  $T_g$  values calculated at 100 s.

A shift of the curves can be seen in Figure 8 and the corresponding  $T_g$ 's in Table 8 toward the oil, for all the systems as the amount of oil increases. Based on Fox's inverse rule of perfect mixtures:<sup>51–53</sup>

$$1/T_g^{\text{mix}} = W_{\text{oil}}/T_g^{\text{oil}} + W_{\text{Polymer}}/T_g^{\text{Polymer}} \quad (4)$$

a prediction of expected  $T_g$  shifts can be derived as given in Table 8 as well. In the present case, the oil is treated as an oligomeric component, based on the fact that the TDAE oil follows VFT behavior in Figure 8. The predicted values are in good agreement with the values derived from the use of a single HN equation to fit the dielectric spectra. It demonstrates that not only the pure polymers S-SBR and BR with oil, but also the S-SBR/BR blends with oil can be treated as a two-component system of the blend and the oligomeric TDAE oil. This is a strong indication for a homogeneous distribution of the oil within the blends.

To explore the effect of the TDAE oil in more detail, the single, broad dielectric loss peak must be further de-convoluted to the individual contributions of both S-SBR and BR polymers in the blend.

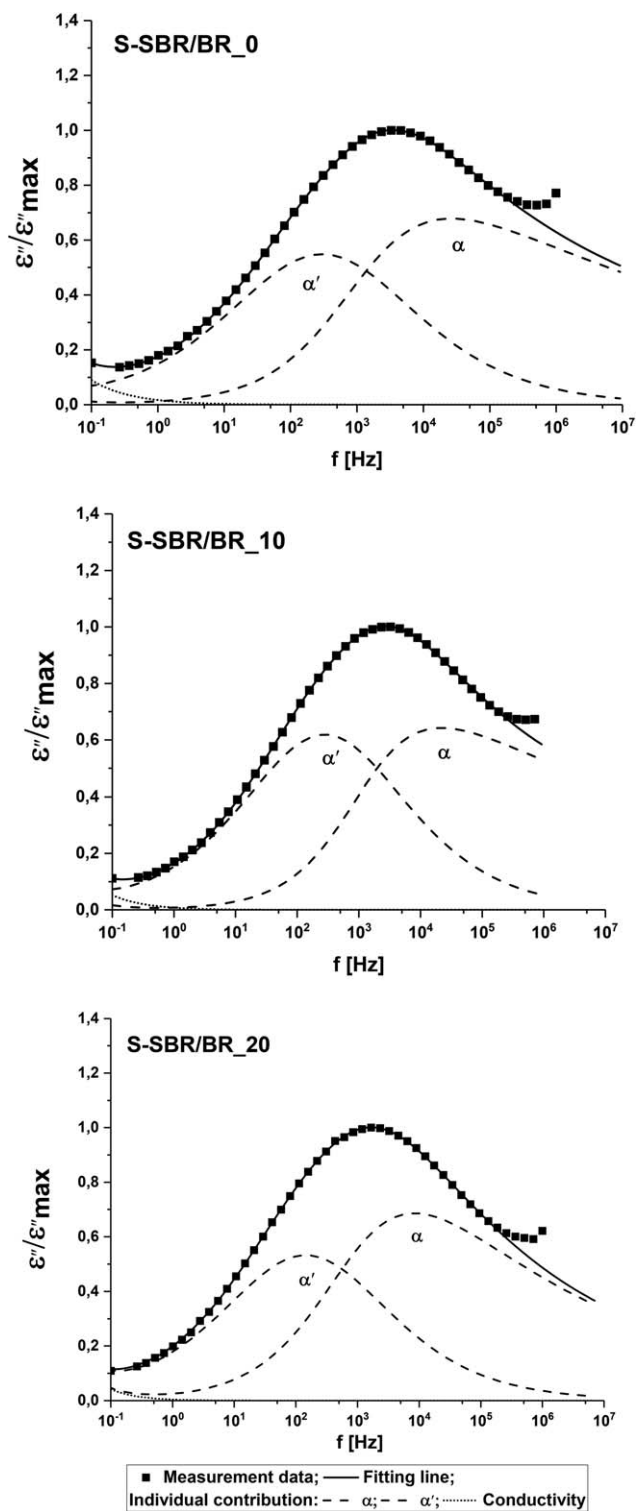


**FIGURE 9** Normalized deconvolution results from fitting of the  $\alpha'$  and  $\alpha$  processes using 2 HN equations at  $T = -30\text{ }^\circ\text{C}$  for the blends: S-SBR/BR\_0, S-SBR/BR\_10, and S-SBR/BR\_20.

### Two HN Equations Based Fittings for the Blends

To resolve the individual contributions of the S-SBR and BR components to the single, broad dielectric loss  $\epsilon''$  peak of the blends, a fitting protocol using two HN-equations was

applied.<sup>26,54</sup> Blending modifies the response of the individual S-SBR and BR components such that they may experience a distinct relaxation environment in the blended state, which can be fitted as individual contributions.<sup>26</sup>

The fittings were performed with the aim of finding two relaxation processes which are referred to as  $\alpha$  for fast and  $\alpha'$  for slow. At the selected temperature  $T = -30\text{ }^\circ\text{C}$  the dielectric loss  $\epsilon''$  is clearly observable as a well-resolved peak of about six decades in the frequency window (Fig. 9). The dielectric loss  $\epsilon''$  can be de-convoluted into two individual relaxation processes depicted as dashed lines. A conductivity contribution, shown as dotted line, was used in the fitting protocol to achieve a better fit of the low frequency tail of the dielectric spectra. The  $\alpha$  and  $\alpha'$  relaxations are assigned as the fast and the slow processes, respectively, in decreasing order of frequency, related to a BR-rich and a blend-rich environment.

The relaxation parameters:  $\Delta\epsilon_{(\alpha)}$ ,  $\Delta\epsilon_{(\alpha')}$ ,  $b$ ,  $b'$ ,  $c$ ,  $c'$ ,  $\tau_{\text{HN}(\alpha)}$ , and  $\tau_{\text{HN}(\alpha')}$  (where ' refers to the  $\alpha'$ -process) for each

**TABLE 9** HN-Fitting Parameters for the De-Convolutd Relaxation Spectra of S-SBR/BR Blends with Varying Concentrations of TDAE

Compound	S-SBR/BR_0	S-SBR/BR_10	S-SBR/BR_20
$T = -40\text{ }^\circ\text{C}$			
$\Delta\epsilon_{\alpha}$	0.22	0.60	0.24
$\Delta\epsilon_{\alpha'}$	0.11	0.24	0.18
$\tau_{\text{HN}(\alpha)}$ (s)	$1.14 \times 10^{-3}$	$1.71 \times 10^{-3}$	$1.85 \times 10^{-3}$
$\tau_{\text{HN}(\alpha')}$ (s)	$6.31 \times 10^{-3}$	$1.67 \times 10^{-2}$	$1.91 \times 10^{-2}$
$b$	0.58	0.54	0.53
$b'$	0.38	0.22	0.39
$c$	0.11	0.42	0.19
$c'$	1	0.97	0.80
$T = -30\text{ }^\circ\text{C}$			
$\Delta\epsilon_{\alpha}$	0.25	0.64	0.26
$\Delta\epsilon_{\alpha'}$	0.09	0.26	0.16
$\tau_{\text{HN}(\alpha)}$ (s)	$1.52 \times 10^{-4}$	$1.51 \times 10^{-4}$	$1.76 \times 10^{-4}$
$\tau_{\text{HN}(\alpha')}$ (s)	$5.87 \times 10^{-4}$	$8.68 \times 10^{-4}$	$9.56 \times 10^{-4}$
$b$	0.63	0.65	0.65
$b'$	0.44	0.49	0.44
$c$	0.11	0.14	0.15
$c'$	1	0.90	0.89
$T = -20\text{ }^\circ\text{C}$			
$\Delta\epsilon_{\alpha}$	0.27	0.72	0.30
$\Delta\epsilon_{\alpha'}$	0.07	0.20	0.12
$\tau_{\text{HN}(\alpha)}$ (s)	$2.49 \times 10^{-5}$	$3.30 \times 10^{-5}$	$3.59 \times 10^{-5}$
$\tau_{\text{HN}(\alpha')}$ (s)	$9.30 \times 10^{-5}$	$1.18 \times 10^{-4}$	$1.44 \times 10^{-4}$
$b$	0.71	0.73	0.72
$b'$	0.52	0.53	0.53
$c$	0.10	0.12	0.14
$c'$	1	1	0.96

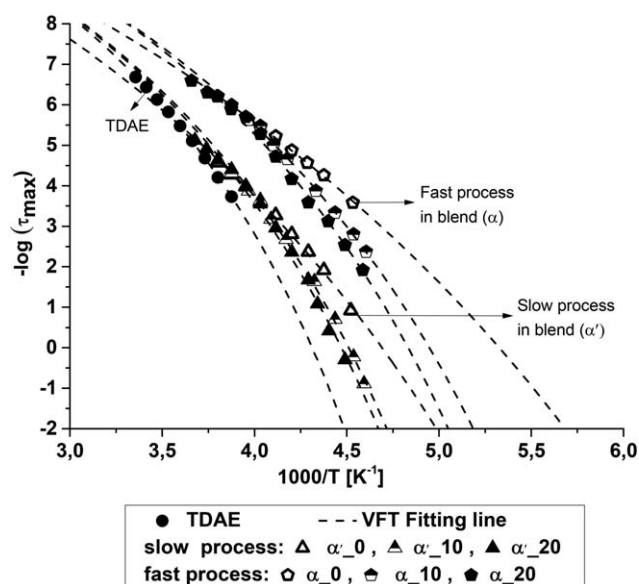


**FIGURE 10** Temperature dependence of the average relaxation times of: TDAE;  $\alpha$  and  $\alpha'$  processes for the blends: S-SBR/BR<sub>0</sub>, S-SBR/BR<sub>10</sub>, and S-SBR/BR<sub>20</sub>.

contribution are shown in Table 9 for selected temperatures of  $-40$ ,  $-30$ , and  $-20$  °C. Figure 10 shows  $\tau_{\max}$  for the  $\alpha$  and  $\alpha'$  relaxation processes plotted as a function of the inverse temperature. The relaxation time curves of the two processes are located apart from each other and seem to converge at higher temperatures, a characteristic feature of the segmental dynamics of polymeric chains as well as of VFT curves, due to the cooperative nature of the segmental relaxations.<sup>54</sup> This trend is observed independent of the amount of oil present in the blends. The effective  $T_g$  ( $T_g^{\text{eff}}$ ) of the fast and the slow processes in the blend is subsequently calculated as the temperature at  $\tau_{\max} = 100$  s ( $\sim 10^{-2}$  Hz), as listed in Table 10. The  $T_g^{\text{eff}}$  corresponding to  $\tau_{\max} = 1$  s ( $\sim 1$  Hz) are also reported in Table 10, although as commented in the previous section, all comparisons will be made based on the convention of 100 s.

#### S-SBR/BR Blend Without Oil

For the blend without oil (S-SBR/BR<sub>0</sub>), the value of  $T_g^{\text{eff}}$  of the slow  $\alpha'$  process ( $-72$  °C in Table 10) is strikingly similar to the  $T_g$  of the total blend ( $-74$  °C in Table 8), whereas the  $T_g^{\text{eff}}$  of the fast  $\alpha$  process ( $-97$  °C in Table 10) is closer to the  $T_g$  of BR ( $-111$  °C in Table 8). These observations indicate that the fast  $\alpha$  process is the response from the more mobile BR segments trying to dissociate from the slower  $\alpha'$  process, which is associated with the blend environment (S-SBR/BR). This can be corroborated with the theories on dynamical heterogeneities of miscible blends. For instance, the Lodge and McLeish (LM) model states that in a miscible mixture of a copolymer (AB) and a homopolymer (A), the lower  $T_g$  component tends to experience its own inherent  $T_g$ , whereas the higher  $T_g$  component tends to experience a blend environment, based on self-concentration of the like

segments.<sup>38</sup> Moreover, in the temperature domain curves, it can also be seen that at high frequencies the BR component of the blends experiences almost the same  $T_g$  as the BR (see Fig. 6). Similarly, on the frequency domain curves, it is observed that the main relaxation of the blends is seen to start at  $-60$  °C and end at  $-20$  °C (see Fig. 7). It is clear evidence that the relaxation of the blends lies in between the relaxation of the BR and S-SBR. At lower temperatures like  $-80$ / $-70$  °C (closer to the  $T_g$  of BR) there is a well-defined small relaxation peak on the right side while the main relaxation peak is still seen to be evolving on the left side. The small relaxation peaks are located in frequency at the same location as for pure BR (compare Figs. 4 and 7). Since the ending at  $-20$  °C is close to the location in frequency to the S-SBR counterpart but does not exactly correspond to it, this can be assigned to the contribution of the blended S-SBR and BR chains. Therefore, based on this it is justified to de-convolute the blend dynamics into two processes: one that experiences a predominantly BR environment and the other one that experiences a blend environment.

#### S-SBR/BR Blends with Oil

For the blends with oil, the general trend is that both the  $\alpha$  and  $\alpha'$  processes show longer relaxation times with increasing amounts of oil, which can be expected since the TDAE oil has slower relaxation dynamics compared to the blends. This effect can most clearly be seen in Figure 10. A clear shift toward higher  $T_g^{\text{eff}}$  for both the  $\alpha$  and  $\alpha'$  processes is observed as oil content increases, the degree of shift being more pronounced for the  $\alpha$  process as compared to the  $\alpha'$  process (see Table 10). The fast  $\alpha$ -process originates from the relaxation of BR segments surrounded predominantly by like-segments and oil. This means that the  $\alpha$  process may be affected by the presence of TDAE oil molecules in a similar way as pure BR. From the effect of TDAE oil on pure polymers, it was already seen that there is a larger effect of addition of TDAE oil on the  $T_g$  of BR than on the of pure S-SBR. A simple explanation to this is the mere difference in  $T_g$  of the BR and oil versus the  $T_g$  of S-SBR and the oil. A more in-depth explanation is that the inherent free volume associated with BR due to its linearity is smaller compared to that of S-SBR due to the bulky styrene-groups and variety of

**TABLE 10**  $T_g^{\text{eff}}$  at  $\tau_{\max} = 100$  s and 1 s of the  $\alpha$  and  $\alpha'$  Processes, Experimentally Obtained from BDS Measurements

Compound		$T_g^{\text{eff}}$ (100 s) (°C)	$T_g^{\text{eff}}$ (1 s) (°C)	$\Delta T_g^{\text{eff}}$ (100 s) (°C)
S-SBR/BR <sub>0</sub>	$\alpha$	-97	-85	-
	$\alpha'$	-72	-60	-
S-SBR/BR <sub>10</sub>	$\alpha$	-80	-71	17
	$\alpha'$	-61	-51	11
S-SBR/BR <sub>20</sub>	$\alpha$	-75	-66	22
	$\alpha'$	-59	-49	13

$\Delta T_g^{\text{eff}}$  is calculated with regard to S-SBR/BR<sub>0</sub>.

microstructures, which means that addition of TDAE oil causes a higher disruption in the relaxation dynamics of BR, whereas in the case of S-SBR most of the TDAE oil can accommodate in the existing free volume without causing much difference from its relaxation dynamics. This explains why a relatively bigger effect of the oil can be noted for the  $\alpha$  process on Table 10. However, the observed effect is larger than the effect on pure BR, which is due to the contribution of the surrounding blended chains. The effect of oil on the  $\alpha'$  process is smaller but not comparable to the effect on S-SBR, which further re-confirms that the  $\alpha'$  process is the contribution of the blended chains rather than only S-SBR from the blends.

## CONCLUSIONS

The studied S-SBR/BR (50/50) blends with and without TDAE oil are miscible blends, as confirmed by the presence of a single glass transition signal observed by DSC, DMA, and also in BDS. Dynamic heterogeneities due to concentration fluctuations within these blends manifest themselves as broadening of the glass-to-rubber transition of the blends, as seen with all three techniques.

Temperature domain BDS measurements were used to clarify the thermorheological behavior of the blends. A change in frequency dependence of the blends was observed: from thermorheological simplicity up to  $10^3$  Hz to thermorheological complexity from  $10^4$  Hz onwards. This demonstrates that the dynamic heterogeneities originate from the smallest segmental motions of the butadiene moieties in the S-SBR and BR components. Frequency domain BDS measurements were further analyzed using fitting protocols based on the use of the HN-principle: (i) one HN equation for the pure polymers and the blends, to find that Fox's inverse rule of mixtures complies with the observed shifts in  $T_g$  for all compounds, upon addition of the oligomeric TDAE oil; ii) two HN equations, to de-convolute the single, broad dielectric loss  $\epsilon''$  peak of the blends into a fast  $\alpha$  and a slow  $\alpha'$  process. The de-convolution showed: (i) the fast  $\alpha$  process is the contribution of dissociated BR segments from the slower blended S-SBR and BR segments, forming the slow  $\alpha'$  process; (ii) there is larger effect of TDAE oil on the fast  $\alpha$  process coming from BR-segments only, similar to the effect of the oil on BR. BDS turns out to be a powerful tool to elucidate the intricacies of the miscible blend dynamics and the effect of extender oil thereon.

## ACKNOWLEDGMENTS

The authors are indebted to H&R Ölwerke Schindler GmbH (Hamburg, Germany) for their scientific, financial, and materials support of the current project as well as the permission to publish this work. M. Hernández acknowledges the European Commission for a Marie Curie Fellowship (PIEF-GA-2013-623379). The authors also acknowledge J. Bijleveld (TU Delft) for the DSC measurements.

## REFERENCES AND NOTES

- 1 K. Fujimoto, N. Yoshimiya, *Rubber Chem. Technol.* **1968**, *41*, 669.
- 2 T. Inoue, F. Shomura, T. Ougizawa, K. Miyasaka, *Rubber Chem. Technol.* **1985**, *58*, 873.
- 3 N. Yoshimiya, J. Fujimoto, *Rubber Chem. Technol.* **1969**, *42*, 1009.
- 4 I. Furata, I. Hattori, F. Tsutsumi, In *Rubber Chemistry and Technology*, Proceedings of the annual spring meeting of American Chemical Society: Rubber Division, Las Vegas, Nevada, U.S.A., May 29–June 1, 1990, Rubber Division, American Chemical Society, Inc.: U.S.A., **1990**.
- 5 R. Rauline, (Generales des Etablissements Michelin-Michelin & Cie), U.S. Patent 5,227,425, July 13, 1993; E.P. 0501227A1, September 2, **1992**.
- 6 M. Sato, W.K. Dierkes, N. Amino, A. Blume, International Rubber Conference, Kitakyushu, Japan, Oct 24–28, 2016; The Society of Rubber Science and Technology: Japan, **2016**.
- 7 P. A. Marsh, A. Voet, L. D. Price, *Rubber Chem. Technol.* **1967**, *40*, 359.
- 8 P. A. Marsh, A. Voet, L. D. Price, T. J. Mullens, *Rubber Chem. Technol.* **1968**, *40*, 344.
- 9 S. Sakurai, T. Izumitani, H. Hasegawa, T. Hashimoto, C. C. Han, *Macromolecules* **1991**, *24*, 4844.
- 10 C. M. Roland, *Macromolecules* **1987**, *20*, 2557.
- 11 S. Shenogin, R. Kant, R. H. Colby, S. K. Kumar, *Macromolecules* **2007**, *40*, 5767.
- 12 Y. Hirose, O. Urakawa, K. Adachi, *Macromolecules* **2003**, *36*, 3699.
- 13 S. A. Madbouly, *Polymer* **2002**, *34*, 515.
- 14 J. Colmenero, A. Arbe, *Soft Matter* **2007**, *3*, 1474.
- 15 W. G. F. Sengers, M. Wübbenhorst, S. J. Picken, A. D. Gotsis, *Polymer* **2005**, *46*, 6391.
- 16 D. Boese, F. Kremer, *Macromolecules* **1990**, *23*, 829.
- 17 B. B. Sauer, P. Avakian, G. M. Cohen, *Polymer* **1992**, *33*, 2666.
- 18 S. Cervený, R. Bergman, G. A. Schwartz, P. Jacobsson, *Macromolecules* **2002**, *35*, 4337.
- 19 V. M. Litvinov, *Macromolecules* **2006**, *39*, 8727.
- 20 K. Saalwächter, A. Heuer, *Macromolecules* **2006**, *39*, 3291.
- 21 Y. He, T. R. Lutz, M. D. Ediger, *Macromolecules* **2004**, *37*, 9889.
- 22 H. Luo, M. Klüppel, H. Schneider, *Macromolecules* **2004**, *37*, 8000.
- 23 K. Saalwächter, M. Klüppel, H. Luo, H. Schneider, *Appl. Magn. Reson.* **2004**, *27*, 401.
- 24 G. C. Chung, J. A. Kornfield, S. D. Smith, *Macromolecules* **1994**, *27*, 964.
- 25 J. O'Brien, E. Cashell, G. E. Wardell, V. J. McBrierty, *Macromolecules* **1976**, *9*, 653.
- 26 S. Zhang, P. Painter, J. Runt, *Macromolecules* **2002**, *35*, 9403.
- 27 A. Algeria, J. Colmenero, K. L. Ngai, C. M. Roland, *Macromolecules* **1994**, *27*, 4486.
- 28 K. L. Ngai, D. J. Plazek, In *Physical Properties of Polymers Handbook*, 2nd ed.; J. E. Mark, Ed.; Springer: New York, **2007**; Chapter 26, pp 455–478.
- 29 G. Heinrich, H. B. Dümmler, *Rubber Chem. Technol.* **1998**, *71*, 53.
- 30 T.-L. Cheng, A.-C. Su, *Polymer* **1995**, *36*, 73.
- 31 J. M. Massie, R. C. Hirst, A. F. Halasa, *Rubber Chem. Technol.* **1993**, *66*, 276.

- 32 L. Mandelkern, In *Crystallization of Polymers*; Cambridge University Press: Cambridge, **2004**; Vol. 2, Chapter 9, pp 1–204.
- 33 A. J. Marzocca, S. Cerveny, J. M. Méndez, *Polym. Int.* **2000**, *49*, 216.
- 34 P. Shi, R. Schach, E. Munch, H. Montes, F. Lequeux, *Macromolecules* **2013**, *46*, 3611.
- 35 G. Teysseck, S. Mezghani, A. Bernes, C. Lacabanne, In *Dielectric Spectroscopy of Polymeric Materials*; J. P. Runt, J. J. Fitzgerald, Eds.; American Chemical Society: Washington, DC, **1997**; Chapter 8, pp 227–258.
- 36 A. Schönhals, In *Broadband Dielectric Spectroscopy*; F. Kremer, A. Schönhals, Eds.; Springer, Berlin Heidelberg GmbH, **2003**; Chapter 7, pp 225–286.
- 37 R. Colby, J. Lipson, *Macromolecules* **2005**, *38*, 4919.
- 38 T. Lodge, T. McLeish, *Macromolecules* **2000**, *33*, 5278.
- 39 A. Rathi, *Process-Design for Tire Tread Compounds with Good Compatibility to Mineral-Based Process Oils*. PDEng. Thesis, University of Twente, Enschede, NL, June **2016**.
- 40 C. M. Roland, K. L. Ngai, *Macromolecules* **1991**, *24*, 2261.
- 41 K. L. Ngai, D. J. Plazek, R. W. Rendell, *Rheol. Acta* **1997**, *36*, 307.
- 42 K. L. Ngai, C. M. Roland, *Rubber Chem. Technol.* **2004**, *77*, 579.
- 43 S. Havriliak, S. Negami, *Polymer* **1967**, *8*, 161.
- 44 R. Richter, C. A. Angell, *J. Chem. Phys.* **1998**, *108*, 9016.
- 45 H. Vogel, *Phys. Z.* **1921**, *22*, 645.
- 46 G. S. Fülcher, *J. Am. Ceram. Soc.* **1925**, *8*, 339.
- 47 G. Tammann, W. Hesse, *Z. Anorg. Allg. Chem.* **1926**, *156*, 245.
- 48 C. A. Angell, *Polymer* **1997**, *38*, 6261.
- 49 C. A. Angell, *J. Non-Crystal. Solids* **1991**, *131–133*, 13.
- 50 K. L. Ngai, D. J. Plazek, *Rubber Chem. Technol.* **1995**, *68*, 376.
- 51 T. G. Fox, *Bull. Am. Phys. Soc.* **1956**, *1*, 123.
- 52 A. Rathi, M. Hernández, W. K. Dierkes, C. Bergmann, J. Trimbach, A. Blume, *Kautsch. Gummi Kunstst.* **2016**, *69*, 22.
- 53 A. Petchkaew, K. Sahakaro, J. W. M. Noordermeer, *Kautsch. Gummi Kunstst.* **2013**, *66*, 43.
- 54 M. Hernández, T. A. Ezquerro, R. Verdejo, M. A. López-Manchado, *Macromolecules* **2012**, *45*, 1070.